Aust. J. Phys., 1986, **39**, 35–55

The LT-4 Tokamak. II*
MHD Activity

A. D. Cheetham,[A,B] *S. M. Hamberger,*[A] *J. A. How,*[A,B] *H. Kuwahara,*[A,C]
A. H. Morton[A] *and L. E. Sharp*[A]

[A] Plasma Research Laboratory, Research School of Physical Sciences,
Australian National University, G.P.O. Box 4, Canberra, A.C.T. 2601.
[B] Present address: JET Joint Undertaking, Abingdon, OX14 3EA, U.K.
[C] Present address: University of Saskatchewan, Saskatoon, SK 57N OWO, Canada.

Abstract

An extensive experimental program has been carried out on the MHD activity occurring in the LT-4 plasma during ohmic heating discharges, under a wide range of reproducible conditions, for $3 \cdot 6 > q(a) > 2 \cdot 5$. Perturbations are studied by using large arrays of individually monitored magnetic coils, distributed both poloidally and toroidally, and two toroidally separated soft X-ray poloidal arrays. The results show that the behaviour can be broadly classified into four distinct regimes within each of which the observable MHD phenomena are remarkably reproducible, and whose boundaries can be very well described by the single parameter $q(a)$. Although most of the observations conform with those on other tokamaks, some appear inconsistent with the usual interpretation, for example, the assumption of rigid toroidal rotation. Further, while internal $m/n = 1/1$ and $m = 0$ sawteeth activity at the $q = 1$ surface are clearly defined, the magnetic signals usually ascribed to a 2/1 mode when $q(a) \leqslant 3$ are clearly shown to have a predominant 3/1 structure, while activity at the $q = 2$ surface appears relatively weak.

1. Introduction

The LT-4 tokamak system, its principal diagnostics and mode of operation have already been presented (Bell *et al.* 1984, hereafter referred to as Part I). In the present paper we describe the methods and results of an investigation into the large scale fluctuations of the tokamak plasma which are known to play an important role in confinement (Furth 1975). These fluctuations are commonly described in terms of a magnetohydrodynamic (MHD) model, since they can be described, at least to a first approximation, by MHD theory (see e.g. Wesson 1978), although recently some doubt has been cast on the adequacy of such a description (see e.g. Thyagaraja and Haas 1983, who suggested that at least a two-fluid treatment is necessary to describe fluctuation phenomena under typical tokamak conditions).

It has long been known that the MHD equilibrium of a tokamak is subject to various forms of instability whose growth rates depend on the local values of the plasma pressure gradient, magnetic shear, current density, etc. (see e.g. Mirnov and Semenov 1971; Hosea *et al.* 1971; Bowers *et al.* 1971). These give rise to perturbations which have the general form (in the laboratory frame)

$$\xi = \xi_0 \exp\{\mathrm{i}(m\theta - n\phi + \omega t)\}$$

with helical structures which generally are most pronounced on or close to those

* Part I, *Aust. J. Phys.*, 1984, **37**, 137.

0004-9506/86/010035$02.00

surfaces at some radius r where the field line helicity matches that of the mode. If m and n are small integers, these are known as 'rational surfaces' and satisfy the condition $q(r) = m/n$. The value of q at the plasma boundary, $r = a$, is often called the 'safety factor' (for historical reasons), while m and n are respectively referred to as the poloidal and toroidal mode numbers. Since for our purposes we are mainly interested in $q(a) \leqslant 4$, the most important modes of concern here are $(m = 3)/(n = 1)$, resonant on the $q = 3$ surface, 2/1* on $q = 2$, and 1/1 associated with $q \leqslant 1$. Some work has argued that the higher order toroidal mode 3/2 (at $q = 1 \cdot 5$) is of significance in certain nonlinear processes which involve coupling between other modes (see e.g. Waddell *et al.* 1979).

The precise nature of the instabilities and the resultant perturbations depend strongly on the actual radial profiles of the various plasma parameters. For instance, if the current density near the hot centre of the plasma is sufficiently high that $q(0) < 1$, that region can support kink modes (e.g. $m/n = 1/1$) which cause rapid transport away from the centre with consequent flattening of the profile until they are suppressed. This leads to a characteristic relaxation process, known as 'sawteeth' from the shape of the oscillogram of X-ray emission, which clearly indicates the existence of a $q = 1$ surface within the plasma column.

More generally, at each rational surface (e.g. $q = 1, 2, 3$) the finite plasma resistivity may allow tearing modes (Furth *et al.* 1963) to develop, causing the magnetic topology to be changed so as to form helical magnetic flux island structures resonant with the surface. Good descriptions of these phenomena have been given by Bateman (1978) and Wesson (1978).

Of those plasma parameters whose mean local values are perturbed by an MHD mode, two are particularly convenient to observe. The first is the change in current density in the outer region of the plasma associated with the presence of a moving magnetic island, which can be studied, albeit with some ambiguity, by its effect on the local poloidal magnetic field outside the plasma. These are conveniently studied with small magnetic search coils, sometimes referred to as 'Mirnov coils'. The second, which is most useful for observing the hotter, inner parts of the plasma, depends on the mode locally perturbing the plasma temperature and/or density, and thus the soft X-ray (SXR) continuum emission. For obvious reasons such observations are most sensitive in the hotter and denser inner plasma regions. A detailed description of both these types of observation is given in Section 2.

Section 3 describes the principal experimental observations and our attempts to characterize the observed phenomena in terms of the single quantity $q(a)$, i.e. the value of q at the limiter. The results and their interpretation are discussed in Section 4.

Before describing the observations, two points should be emphasized. Firstly, the very phenomena under investigation, which by their nature can grow or decay very rapidly, may themselves have a large effect on the plasma transport properties, and so change those plasma parameters which determine the equilibrium (see Part I). Since the analysis of the spatially resolved data requires a precise knowledge of the plasma position, even quite small changes can cause problems with the interpretation of the fluctuating signals. It is therefore very important that the plasma position control system be sufficiently fast and accurate to maintain a fixed plasma equilibrium

* For convenience and brevity we use the notation m/n to denote a mode with poloidal and azimuthal mode numbers m and n respectively, r_s for the radius at which $q = s$, and ω_{mn} for the observed frequency of a mode m/n.

position. For these reasons the unusually fast and precise feed-back position control system installed on LT-4 makes it particularly suitable for this type of research.

Secondly, these results were obtained during one year of operation (1984) and have been restricted to those shots which produced consistent and reproducible data. Some phenomena described in Section 3 differ qualitatively from those seen under less reproducible conditions during earlier and less systematic investigations. For example (Kuwahara *et al.* 1983; Cheetham *et al.* 1983), the Mirnov coil signals, under plasma conditions not obviously different from those of the present work, had sometimes shown a significantly stronger (even dominant on occasions) 2/1 harmonic content than reported here.

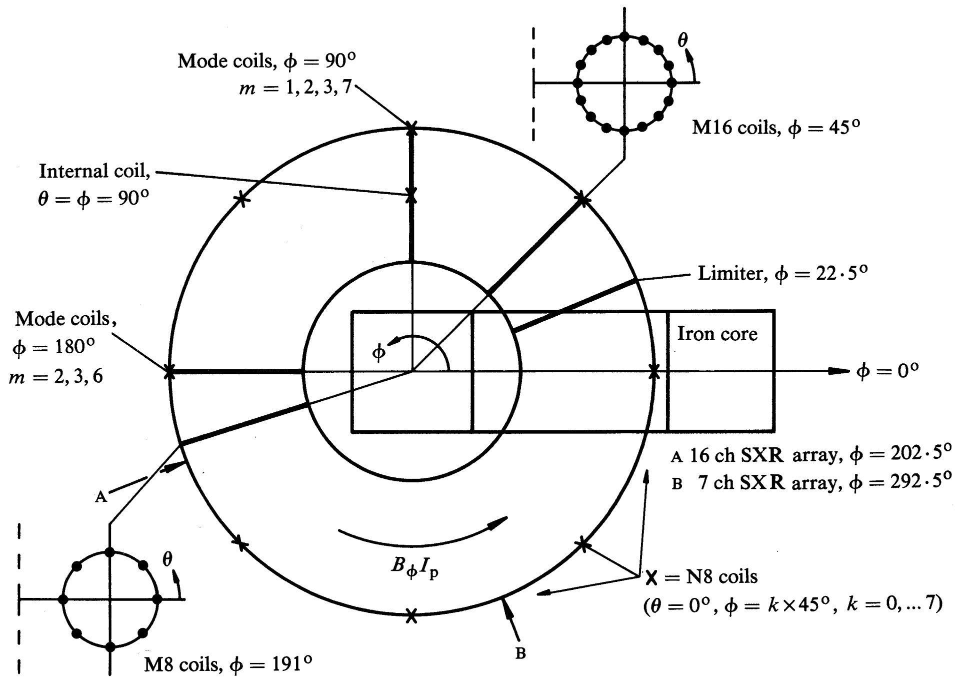

Fig. 1. Plan of LT-4 showing the configuration and positions, relative to the iron core and limiter, of the magnetic pick-up coils and the two soft X-ray detector arrays used for detecting the MHD activity to the iron core and limiter.

2. Diagnostics

A general description of the main diagnostic and data handling systems is given in Part I, while the data system itself has been described more fully by Corbould and How (1984). The following discussion describes in some detail the two diagnostic methods used specifically for the study of the MHD modes, namely arrays of external magnetic pick-up coils and of soft X-ray detectors.

Magnetic Coils

Fig. 1 shows the positions of the various arrays of coils, which are all oriented to respond to the time varying poloidal field components $\dot{B}_\theta$, as mounted around the torus. Two of these arrays are poloidally distributed; one (known as the M16 array) comprises 16 individually monitored separate coils, and the second (M8) of 8 individual coils. Another array (N8) consists of eight coils equally spaced toroidally around the outside of the vessel. The locations of the individual coils are detailed in Fig. 1. Each coil in M16 and N8 consists of 100 turns of 0·35 mm diameter enamelled copper wire wound in two layers on a 6·4 mm diameter plastic former with an effective area of $3{\cdot}73\times10^{-3}$ m^2, while that in M8 consists of 50 turns on a rectangular former, 20×3·18 mm, making an effective area of $3{\cdot}17\times10^{-3}$ m^2.

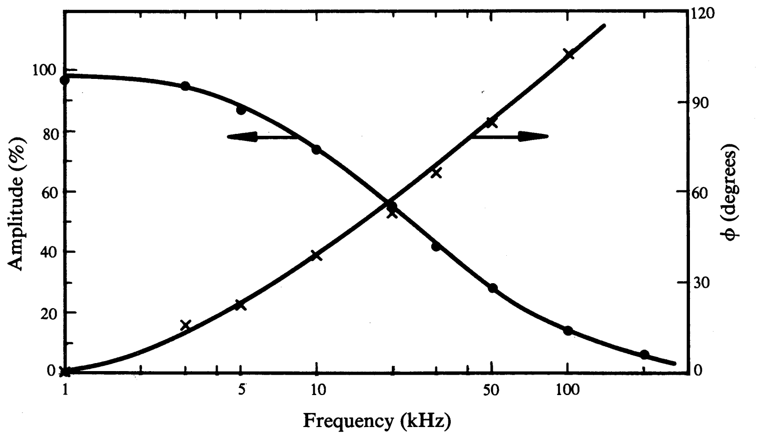

Fig. 2. Frequency response of the vacuum chamber to local B_θ perturbations showing the amplitude and the phase lag ϕ.

The frequency response of the coils and their output circuit is flat (i.e. signal proportional to frequency) up to at least 100 kHz, the highest frequency of interest in this work. However, since the coils are all mounted outside the vacuum vessel (1·4 mm thick Inconel 600) the overall response of the system is affected by the finite penetration time of the fluctuating magnetic fields through the conducting wall. The measured frequency response to local magnetic perturbations is plotted in Fig. 2: it shows that a 30 kHz signal is attenuated by about half, and phase-shifted about 60°. Since the observed MHD activity in LT-4 lies mainly in the range 10–50 kHz it is necessary to make appropriate corrections, for example, when comparing signals at different frequencies.

As a general precaution against missing any significant higher frequency component due to the screening effect of the vessel wall, these are monitored by a further magnetic probe, capable of responding without attenuation to signals up to about 100 kHz and located between the plasma current boundary (as defined by the limiter) and the wall.

As shown in Fig. 1, in addition to the arrays of individually monitored fixed coils there are installed several sets of coils permanently cross-connected electrically so as to respond selectively to specific poloidal harmonics of the external field, namely $m = 1, 2, 3, 6, 7$, the arrangement being based on cylindrical symmetry. Since toroidal effects are important so that, for example, a single helical toroidal mode with poloidal mode number produces signals in the cylindrical system with components $m\pm1$ (Stix 1976), the signals derived from these coil sets are treated as only indicative of the presence of the appropriate mode, and all quantitative information is obtained by analysis of the signals from the individual coil arrays.

The signals from each coil are digitally recorded, normally at 200 kHz sampling rate. Higher rates, up to 2 MHz, can be used for correspondingly shorter durations when greater time resolution is required.

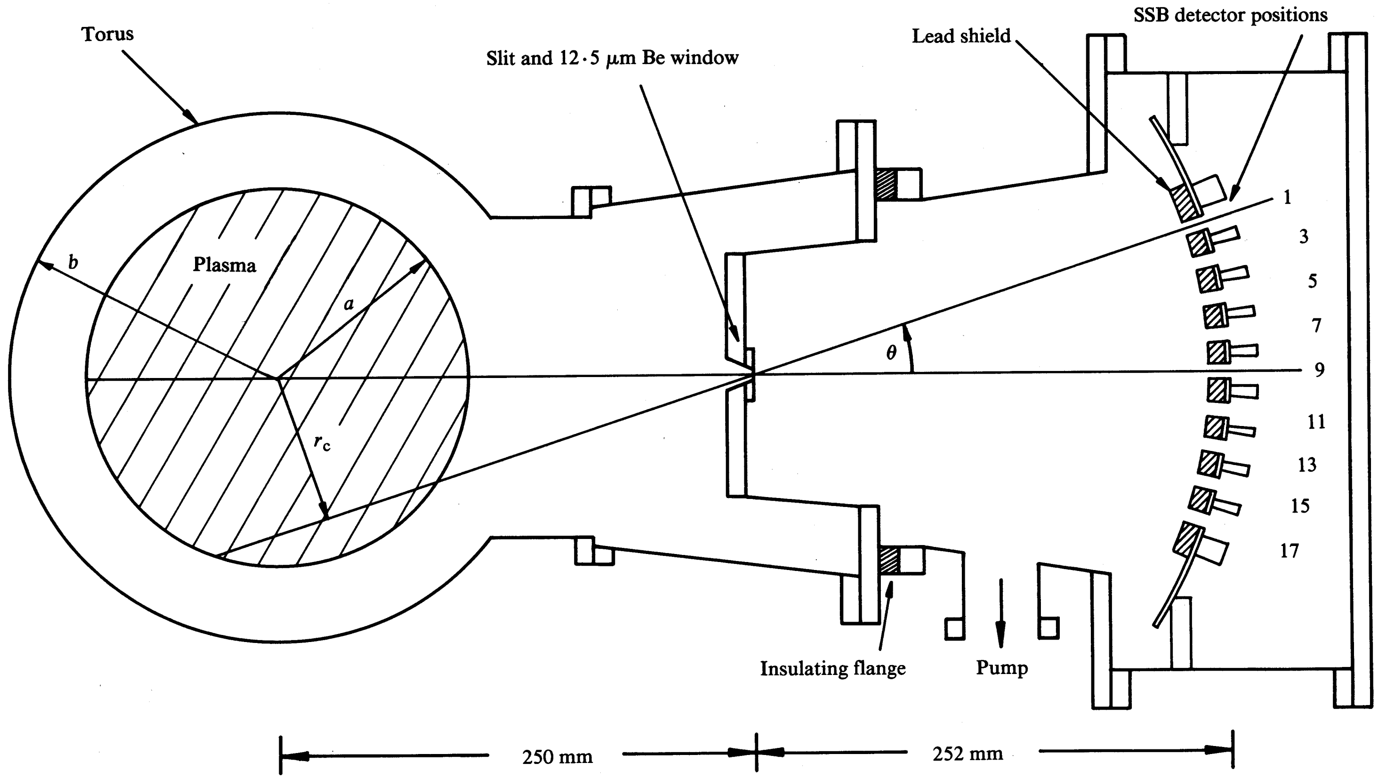

Fig. 3. Schematic diagram of the soft X-ray array on LT-4, showing the plasma radius a, vacuum chamber radius b, and minimum radius of the chord viewed by a diode r_c.

Soft X-ray Emission

The study of MHD modes through their effect on the emission of the soft X-ray continuum is now well established (von Goeler *et al.* 1974). The principal detector array on LT-4, shown schematically in Fig. 3, employs 18 silicon surface barrier detectors (ORTEC Type CA-17-50-100 of 8 mm diameter, 100 μm thickness) which view the plasma through a common window. This consists of a horizontal slit, 4×11 mm, covered with a $12\cdot5$ μm beryllium foil to exclude visible light and most line radiation. Each detector thus views a different chord through the plasma column whose minimum radii (r_c in Fig. 3) are respectively $-8, -7, -6, \ldots, +8, +9$ cm above the median plane of the plasma. The X-ray flux received by each diode is then due to the X-ray emission integrated along the chord for the whole volume viewed by the detector. Since the detector output increases rapidly with both electron temperature and density, the detected signals are heavily weighted by, and can therefore be effectively localized to, the regions of highest temperature and density along the viewing chord, which for monotonically varying profiles means from the region $r = r_c$. The slit width and diode size result in an effective spatial resolution about 16 mm in minor radius. A second array, of essentially similar design but with seven detectors viewing only the lower half of the plasma, is located 90° toroidally from the above array. The location of both arrays are shown as A and B in Fig. 1.

The response of both X-ray systems is limited at low energies by the absorption of the beryllium window (50% transmission at $1\cdot2$ keV) and at high energies by the thickness of the silicon detector (50% response at $10\cdot4$ keV). The relative values of the X-ray signals can be related to plasma temperature and density by starting from the general expression for the X-ray continuum emission spectrum (Wing 1975)

$$I(E) \propto n_e^2\, Z_{\text{eff}} \exp(-E/T_e)/T_e^{\frac{1}{2}},$$

where E is the photon energy, n_e and T_e are the electron density and temperature, and Z_{eff} is the effective charge defined as

$$Z_{\text{eff}} = n_i^2\, Z_i^2/n_e^2,$$

and by allowing for the energy dependence of the detector and absorbing window.

The diode output signals from the 7 channel array are amplified (d.c. to 500 kHz) and recorded simultaneously at both slow and fast sampling rates: the entire pulse is recorded at 5 kHz to enable the slow temporal evolution of the plasma emissivity profile to be examined. By increasing this to 36 kHz the internal relaxations (sawteeth) can be resolved, while for detailed observations of the MHD structure itself it is necessary to record at 200 kHz, after appropriate filtering of the signal to remove the low frequency components (<300 Hz). This fast recording is always synchronized with that of the magnetic signals and, because of limited data storage capacity, is acquired for periods of 20 ms chosen to include a feature of interest. Considerable care is taken to record time accurately in order to maintain chronology of the events recorded on different data aquisition units.

The signals from the 18 channel array are digitized with 12 bit accuracy by means of a Transiac Traq I data acquisition system. The memory allocation for this unit (256 kilo-words) is large enough such that 80 ms of the pulse (which in general includes all features of interest) can be acquired even at the 200 kHz sampling rate.

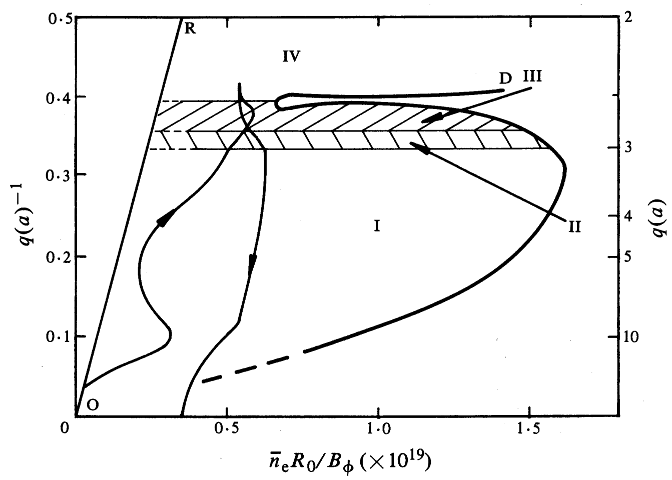

Fig. 4. Hugill diagram for LT-4 showing the important MHD regimes as well as the trajectory of the shot shown in Fig. 5.

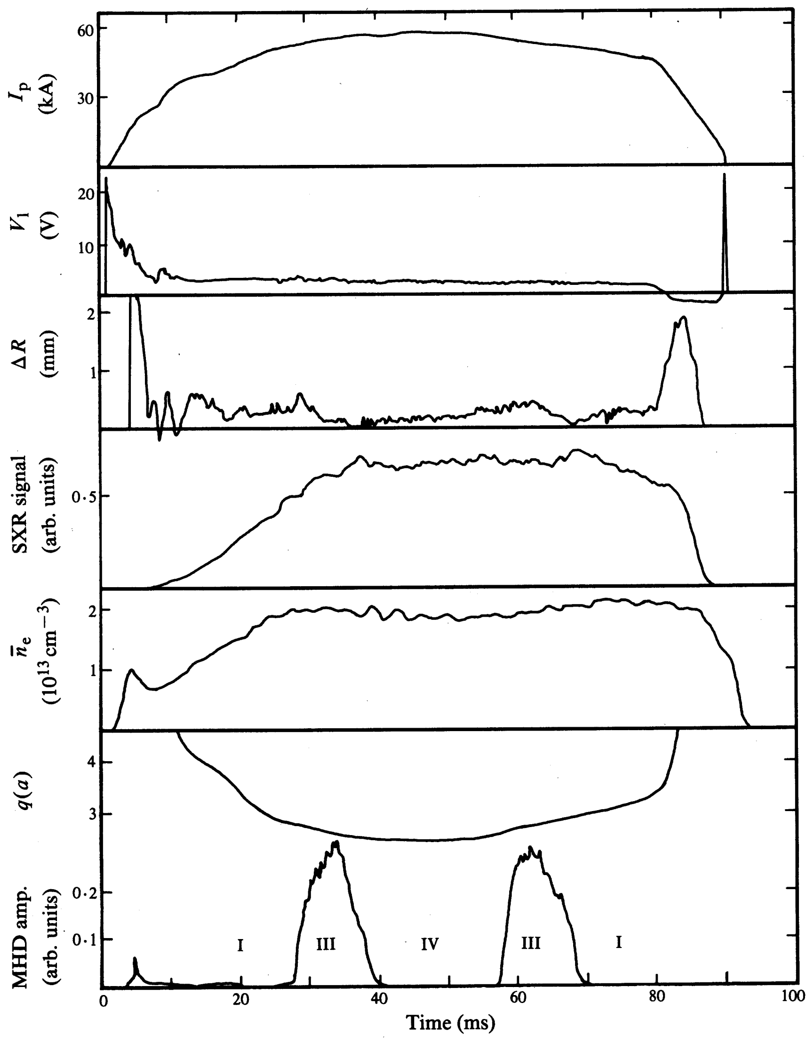

Fig. 5. Signals from a typical shot which passes through all four MHD regimes showing the plasma current, loop voltage, plasma movement, soft X-rays, density, $q(a)$ and MHD amplitude.

In subsequent data analysis the signals are combined, smoothed and Abel inverted to provide the temporal evolution of the radial distribution of X-ray emissivity, and thus to extract, for example, central intensity, emissivity half-width, and vertical plasma position as functions of time.

3. Experiments and Results

The observations described here have all been made within the following range of experimental conditions:

Plasma major radius	$R_0 = 0 \cdot 50$ m
Plasma minor radius	$a = 0 \cdot 095$ m
Toroidal field	$1 \cdot 1 \leqslant B_\phi \leqslant 2 \cdot 1$ T
Plasma current	$40 \leqslant I \leqslant 70$ kA
Pulse duration	~ 100 ms
Mean electron density	$1 \cdot 5 \leqslant \bar{n}_e \leqslant 5 \times 10^{19}$ m^{-3}
Central electron temperature	$200 \leqslant T_e \leqslant 700$ eV
Impurity level	$2 \leqslant Z_{\text{eff}} \leqslant 4$
Safety factor	$2 \leqslant q(a) \leqslant 4$

The range of grossly stable operating conditions can be conveniently described by the so-called 'Hugill diagram' (Fielding *et al.* 1977), as in Fig. 4. This is a normalized plot of plasma current $[q(a)^{-1} \equiv I(\mu_0 R_0/2\pi a^2 B_\phi)]$ against number density $(n_e R_0/B_\phi)$. To the left of the line OR the density is too low to prevent the current being carried mainly or wholly by runaway electrons (Knoepfel and Spong 1979), while to the right of the line OD the density is so high that stable operation is prevented by the disruption of the current channel (for a variety of reasons). The actual lines OD and OR depend at least to some extent on the degree of plasma purity, and thus on the state of vacuum cleanliness, etc.

In actual operation the plasma current is generally under the direct control of the operator, while the density is controlled, as far as is possible within set bounds, by adjusting the rate of hydrogen gas admission ('gas puffing') during the pulse. In order to achieve the desired high density, high current conditions in a tokamak (required for successful tokamak reactor operation), it is necessary that the locus of the operating point (I, n) passes through narrow windows between OR and OD (FT Group 1983) such as that around $q(a) \approx 2 \cdot 5$ shown in Fig. 4. These windows are associated with operating regions characterized by strong MHD activity, such as those marked II and III in Fig. 4. The results which follow are mainly concerned with this type of activity. Waveforms of various quantities obtained during a typical LT-4 discharge are shown in Fig. 5, and the corresponding locus of the operating point in the Hugill diagram plotted in Fig. 4. The density is controlled so that $q(a)$ can be decreased to $2 \cdot 4$ without a disruption. As a result of investigating many such discharges, it has been found that the observable MHD phenomena encountered can be broadly categorized into four kinds, corresponding to four separate regimes, labelled I–IV, which can be characterized by the value of $q(a)$ and all of which occur during the shot of Fig. 5.

In order to study each regime in detail, the toroidal field and plasma current are adjusted to ensure that the appropriate conditions occur while the plasma current is essentially constant, so that conditions remain steady for periods up to 40 ms. Such shots have been recorded for many different conditions and combinations of magnetic field and current within the range indicated above. The four MHD regimes are each described in detail below.

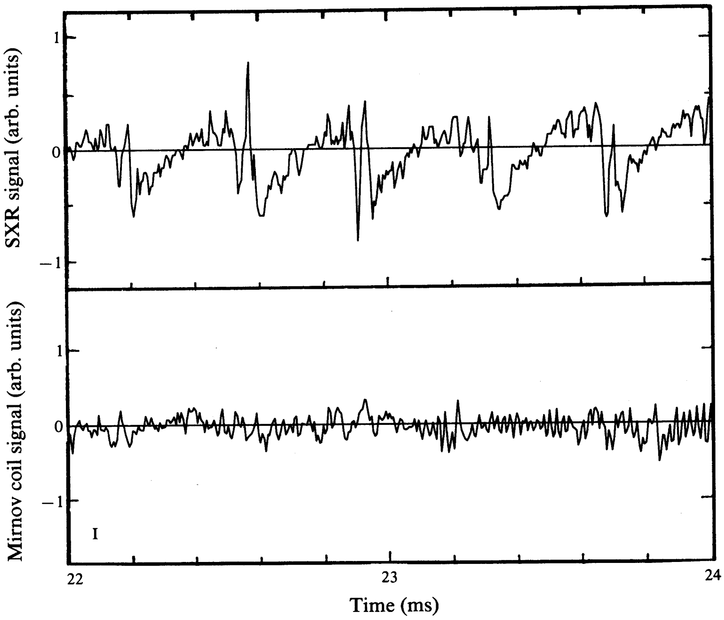

Fig. 6. Magnetic and soft X-ray signals (r = 1 cm) during regime I. The vertical axes are to the same scale as those in Figs 7, 8 and 10.

Regime I: $3{\cdot}6 > q(a) > 2{\cdot}9$

No regular oscillations are seen on the magnetic coil signals, although irregular, weak signals may occur irreproducibly. The SXR signals, however, show strong sawteeth accompanied by precursor oscillations, as seen in Fig. 6, characteristic of a discharge in which $q(0) < 1$. The $q = 1$ surface, at which the sawtooth pattern inverts, is found to occur at $r \approx 3$ cm. By comparing the phases of the oscillatory part of the SXR signal for different radii r_c we find that the regions of high emissivity have $m = 1$ poloidal mode structure. We believe this to indicate the presence of a $m/n = 1/1$ mode on the $q = 1$ surface, as well documented for other tokamaks (Von Goeler *et al.* 1974). Despite the obvious presence of the internal activity, this regime is macroscopically very stable with good confinement properties, and allows relatively high densities to be achieved (Fig. 4).

Regime II: $2{\cdot}9 > q(a) > 2{\cdot}8$

This narrow and usually transient regime is characterized by the presence of small but distinctive oscillations on the magnetic signals (Fig. 7), whose amplitude (at the coils) corresponds to $\tilde{B}_\theta / B_\theta \approx 0{\cdot}05\%$ with frequency typically around 40 kHz. Spatial analysis of the coil signals reveals this to be a mode with $m/n = 3/1$. On the other hand, the SXR signals remain similar to those in regime I with the precursor oscillations increasing in amplitude and having approximately half the frequency of the 3/1 magnetic field signals, i.e. ~ 20 kHz. Although these conditions are regularly seen during the current rise and may remain steady for as long as 40 ms provided $q(a)$ is maintained within the same narrow bounds, unlike the other regimes, it is never observed during the current descent, i.e. following a period in regime III.

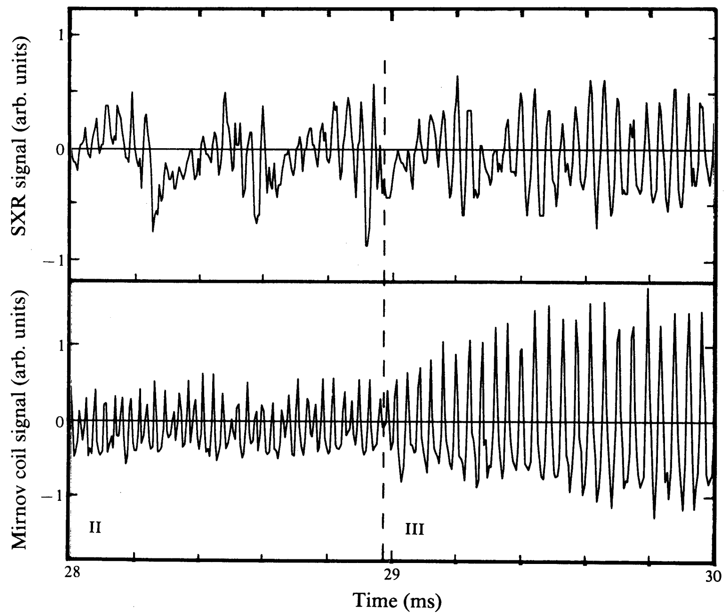

Fig. 7. Magnetic and soft X-ray signals during the transition from regime II to III.

Regime III: $2\cdot 8 > q(a) > 2\cdot 5$

This regime exhibits the most pronounced activity in the outer region of the plasma, as evidenced by the level of the magnetic fluctuations. As $q(a)$ is decreased below $2\cdot 8$ the magnetic signals change quite dramatically, as illustrated in Fig. 7: within one or two cycles the frequency falls roughly to half and locks to that of the SXR signal, i.e. $\sim$ 20 kHz. Simultaneously their amplitude grows until saturating at a level $\tilde{B}_\theta/B_\theta \approx 0\cdot 3\%$ while the now common frequency slowly decreases, sometimes to as low as 12 kHz. Simultaneously, despite the fact that the $q = 3$ surface is outside the plasma column (see Section 4), harmonic analysis of the signals shows that these strong signals have a dominant $(m = 3)/(n = 1)$ structure (see Fig. 14, Section 4), although there is some 2/1 component. The presence of a 2/1 mode at $r \approx 6\cdot 5$ cm can be deduced from the SXR signals (Fig. 15, Section 4, shows the radial dependence of both relative and absolute amplitudes of the SXR fluctuations). As the magnetic fluctuation grows, so does the amplitude of the $m = 1$ SXR signal until it effectively swamps the sawtooth oscillations (Fig. 8).

Macroscopically, the temporal evolution of the SXR emission profile (Fig. 9) shows it to broaden and collapse at the transition from II to III. The central emissivity decreases by up to 70%, while the line-averaged electron density (monitored by interferometry, see Part I) can drop by up to 10%.

At higher densities ($\bar{n}_e R_0/B_\phi > 10^{19}$), as $q(a)$ decreases, the previously steady oscillations themselves exhibit periodic relaxations (Fig. 10) which can be seen on both magnetic and SXR signals. These have periods of several ms, much larger than those of the $q = 1$ sawteeth ($\sim 0\cdot 3$ ms); they appear similar to the phenomena referred to as 'soft disruptions' described by Turner and Wesson (1982), although the latter were observed at larger values of $q(a)$.

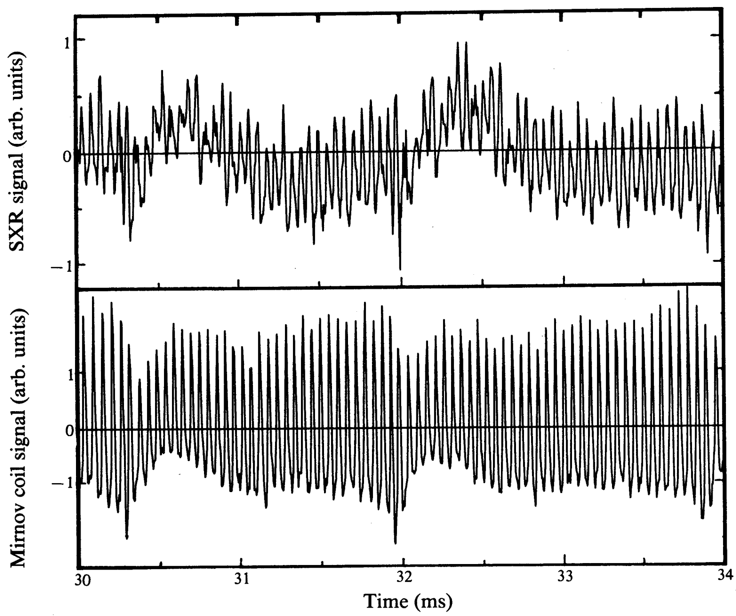

Fig. 8. An example of the relaxations which can occur in regime III. Note that the time window displayed here is twice that shown in Figs 6, 7 and 10.

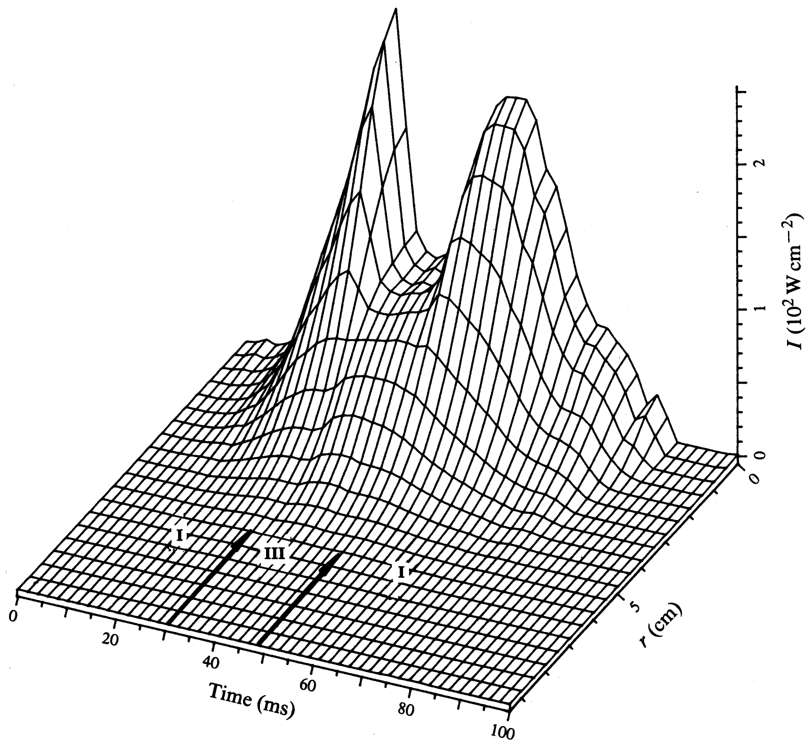

Fig. 9. Temporal evolution of the profile of the soft X-ray flux, showing the effect of the strong regime III activity on the profile. Regime II (not shown) exists for about 1 ms at 29 ms.

At slightly lower densities a further phenomenon of interest sometimes occurs at the edge of the window ($\bar{n}_e R_0/B_\phi \sim 0\cdot7\text{–}0\cdot8\times10^{19}$), in which mode rotation is seen to stop and restart very abruptly and erratically. This behaviour, which usually ends in a disruption, will be described in detail in a separate paper.

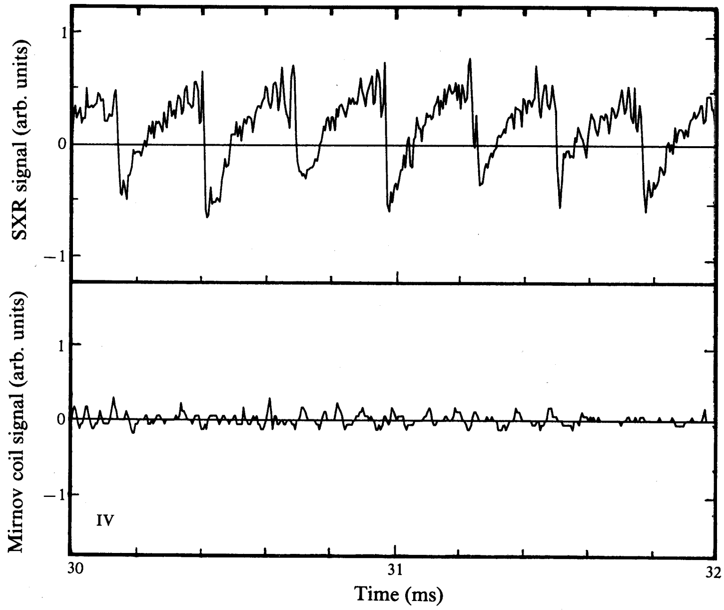

Fig. 10. Magnetic and soft X-ray signals that occur during regime IV.

Regime IV: $q(a) < 2\cdot 5$

As $q(a)$ is reduced below about $2\cdot5$, and provided the density is not too high (see Fig. 4), the magnetic fluctuations fall to a very low level, $\Delta\tilde{B}_\theta/B_\theta \leqslant 0\cdot01\%$, while sawteeth reappear with their accompanying $m = 1$ oscillations at frequency $\sim$20 kHz (Fig. 10).

The SXR emissivity profile generally becomes rather broader than in regime III, with total radiation increased in both the soft X-ray and electron cyclotron harmonic region of the spectrum, indicating higher mean temperatures. It is under conditions such as these that major disruptions are most likely to occur during attempts to decrease $q(a)$ still further. Their appearance and the precise value of $q(a)$ at which they occur are less predictable than the other phenomena described here, and depend sensitively on the impurity level, gas injection rate, and rate of current change (all of which influence the current profile). The lowest value of $q(a)$ achieved so far on LT-4 without disruption (if we exclude non-steady conditions deliberately induced by rapid current ramping) is $q(a) = 2\cdot3$.

The large disruptions in this regime are themselves preceded by a series of minor disruptions (in which smaller plasma energy and poloidal flux losses occur); however, contrary to experience in most other tokamaks, none of these rapid losses appear to be associated with the previous growth to large amplitudes of one or two well-defined, oscillatory low-order modes (e.g. 2/1) (Cheetham *et al.* 1985). The specific details of the actual disruption event and its precursor phase will be the subject of a separate paper.

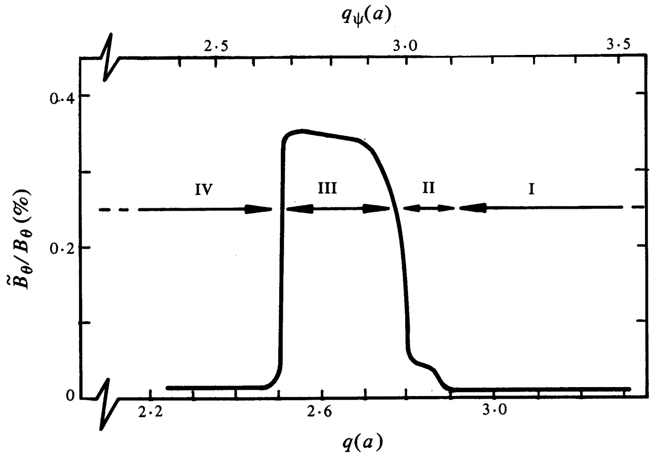

Fig. 11. Maximum MHD amplitude against $q(a)$ showing the four different regimes. The flat top $q(a)$ value was varied from shot to shot and the maximum amplitude was measured in each case.

4. Discussion of Results

The essential features of the results presented in Section 3 are summarized graphically in Fig. 11. This diagram is derived from data taken from about 50 different discharges showing the relation between the amplitude of the externally measured poloidal field fluctuations and the value of $q(a)$, and was obtained as follows. Each measurement was made in one of several sequences of shots in which, for a given plasma current, the toroidal field was successively reduced, this sequence being repeated for different currents. The amplitudes are those for which the activity was saturated, i.e. the signal had reached a steady level, the corresponding values of $q(a)$ in Fig. 11 being calculated from equation (1) (below) by using the measured quantities.

Also indicated in Fig. 11 are the four activity regimes described in Section 3: we find that the critical values of $q(a)$ which separate the regimes remain the same, within experimental uncertainty ($\leqslant 5\%$), throughout the entire range of operating parameters listed in Section 3. It should be noted that regime IV is not accessible to operation at those densities which lie to the right of the window in the Hugill diagram (Fig. 4), i.e. for $\bar{n}_e R_0/B_\phi \geqslant 0 \cdot 6 \times 10^{19}$. By implication, since it is well known that in ohmically heated tokamaks the mean temperature $\bar{T}_e$ is approximately proportional to the current I, the behaviour illustrated in Fig. 11 is insensitive to the temperature.

One factor which is more difficult to control or quantify, and which is known to affect the MHD stability (see Wesson 1978), is the detailed shape of the current density profiles. To the extent that these are affected by such experimental conditions as rate of change of current or gas feed rate, plasma contamination, etc., the Hugill diagram as presented is not unique, and could indeed benefit by the addition of a third axis, for example a form factor such as $q(a)/q(0)$, to reflect this.

In this paper we have followed convention by defining $q(a)$ in its cylindrical approximation:

$$q(a) \equiv 2\pi B_\phi a^2/\mu_0 I R_0 . \tag{1}$$

Strictly, the field line helicity q on a closed magnetic surface should be defined in terms of the variation of toroidal and poloidal fluxes through the surface (see e.g. Bateman 1978, p. 64). However, for the fairly large aspect ratio ($R_0/a \sim 5$) and nearly circular plasma cross sections of LT-4 the difference is not very large: a first-order correction to include toroidicity leads to the expression

$$q_\psi(a) = q(a)(1-a^2/R_0^2)^{-3/2} = 1\cdot 06\, q(a)\,. \tag{2}$$

Finally, before discussing the significance of some of the more interesting results, we should comment on the origin of the oscillatory magnetic signals sometimes referred to as 'Mirnov oscillations'. It is generally agreed that they are caused by perturbations having the form of topologically toroidal magnetic flux islands whose axes are helices lying on or close to the appropriate unperturbed resonant magnetic surface at radius r_s, i.e. with $q(r_s) = m/n$. Regular oscillations in the externally observed signals can arise from motion of such helical structures: for a given mode the frequency measures the appropriate phase velocity in the laboratory frame. The motion is generally (but not universally) believed to be that of the rigid rotation of the plasma column in the toroidal direction. Other possibilities include poloidal rotation, although theoretical arguments suggest this would be heavily damped by collisions (Hassan and Kulsrud 1978), as well as non-rigid, i.e. sheared, toroidal rotation. Also the perturbations may themselves have oscillatory amplitudes and so have a real phase velocity with respect to the plasma.

The amplitude of the observed signal can be related to the half-width δ of the magnetic island at radius r_s through the formula (TFR Group 1982)

$$\delta \approx \left(\frac{2r_s^{2-m}r_{\rm coil}^m}{m}\,\frac{\tilde{B}_\theta}{B_\theta}\right)^{\frac{1}{2}}, \tag{3}$$

where $r_{\rm coil}$ is the radius at which the pick-up coil is located. For example, for $m = 2$ modes in LT-4, $r_{\rm coil} = 14\cdot 5$ cm, $r_s \sim 9\cdot 5$ cm and $\tilde{B}_\theta/B_\theta \sim 0\cdot 003$ corresponds to $\delta \sim 8$ mm.

In the following discussion we attempt to explain the observed phenomena, emphasizing those special features which do not conform to general experience on other tokamaks. For consistency, we follow a sequence of decreasing $q(a)$ from the well-behaved, best-confined conditions of regime I through to the next quiescent phase of regime IV which precedes low-q major disruptions.

Regime I

Fig. 12 shows temperature profile data obtained during conditions typical of regime I, derived from three different diagnostic methods described in Part I, namely Thomson scattering, soft X-ray emission spectrum, and electron cyclotron harmonic emission. Fig. 13 shows the q profile derived from the above data on the usual assumption that the current density is proportional to the electrical conductivity, which in turn is based on Spitzer's formula assuming $Z_{\rm eff}$ independent of r. The presence and location of the $q = 1$ surface at $r_1 \sim 3$ is consistent with the observed X-ray activity [$(m = 1)/(n = 1)$ and sawteeth] described in Section 3. The location of the $q = 2$ and 3 surfaces in the cooler outer regions (at $r_2 \sim 7$ cm and $r_3 \sim 9$ cm respectively) is consistent with the growth, through tearing instability, of only small amplitude islands, and thus weak observed signals.

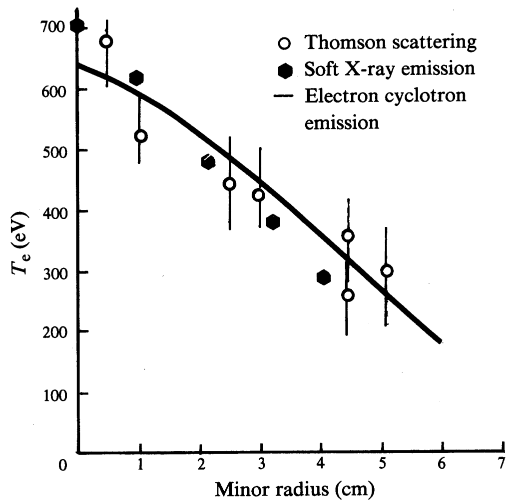

Fig. 12. Typical electron temperature profile $T_e(r)$ obtained during regime I from three diagnostic methods; $I = 60$ kA, $\bar{n}_e = 3{\cdot}5\times10^{13}\,\mathrm{cm}^{-3}$, $B_\phi = 2$ T [$q(a) = 3{\cdot}3$].

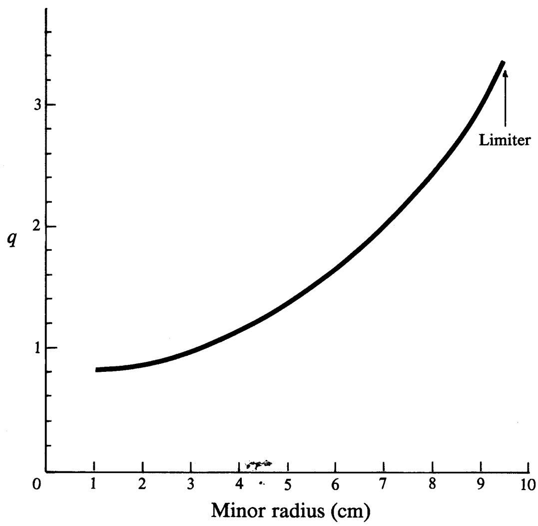

Fig. 13. Profile $q(r)$ derived from the data of Fig. 12.

Transition to Regime II

As the current is increased so that r_2 and r_3 move outwards towards the boundary, modes are excited which, on detailed spatial analysis of the magnetic signals, appear to have strong $m = 3$ and $n = 1$ structure, though with a significant 2/1 component. The structure of the signals can be seen in Fig. 14, where their amplitude is plotted against the pseudo-toroidal coordinates θ and ϕ.

Here the difficulty lies in explaining the large difference in frequency, observed only in regime II, between the magnetic signal originating from the outer regions and that of the X-ray fluctuations from the inner part, which have unambiguously $(m = 1)/(n = 1)$ origin: to be consistent with the widely held belief in rigid toroidal rotation they should have a ratio exactly 2 : 1 if they have respectively toroidal mode numbers $n = 2$ and $n = 1$. However, a detailed comparison shows that the frequencies are neither in the correct ratio (in fact, the ratio changes significantly with time) nor are they locked in phase, as required by rigid rotation. In any case, clear $n = 1$ structure of the higher frequency signal is evident from Fig. 14.

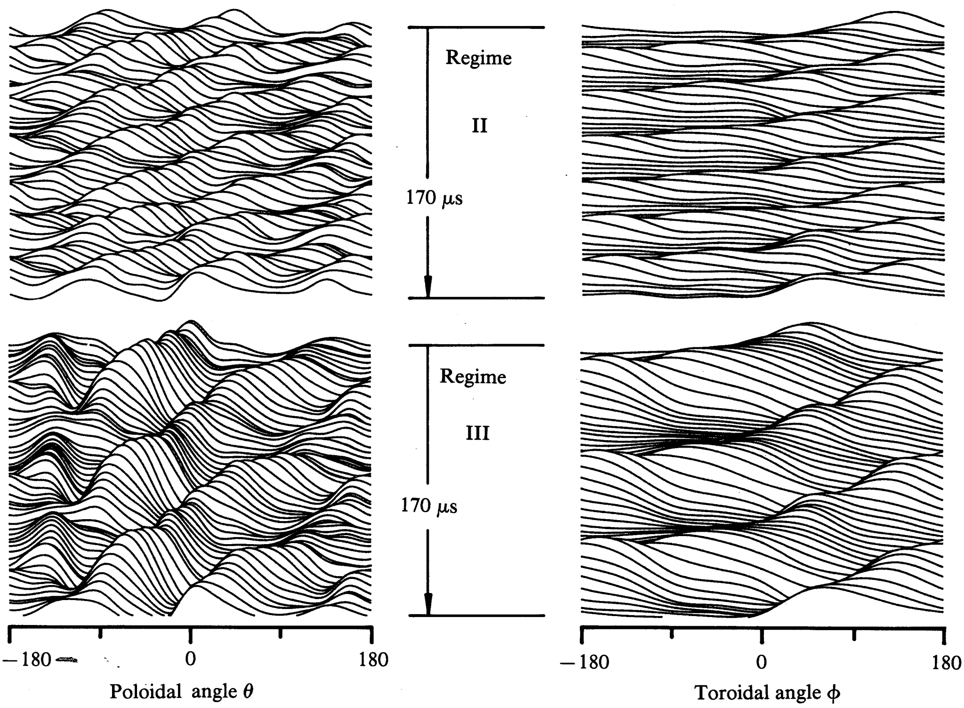

Fig. 14. Spatial structure of the modes in regimes II and III as functions of time. These data show that the mode is $m/n = 3/1$ in both cases, but that the frequency changes on passing from regime II to III.

If we thus rule out rigid toroidal rotation we are left with several other possibilities, either singly or in combination:

(*a*) The plasma rotates rigidly in both toroidal and poloidal directions, with surface velocities V_ϕ and V_θ respectively. Then the observed frequency will be

$$\omega = m V_\theta / r + n V_\phi / R. \tag{4}$$

(*b*) The rotation is purely toroidal, but sheared $[V_\phi = V_\phi(r)]$, so that the $q = 1$ and $q = 3$ surfaces move at different speeds.

(*c*) The perturbations are not frozen into the bulk medium, but move with some finite phase velocity through the plasma.

Possibility (a) can easily be satisfied if we examine data such as that in Fig. 7. Here we have two modes with frequencies $\omega_{11}/2\pi = 26$ kHz and $\omega_{31}/2\pi = 36$ kHz respectively: to satisfy equation (4) requires an azimuthal velocity $V_\phi = 6\cdot6\times10^4$ m s^{-1} combined with a bulk poloidal rotation, slower by a factor of $\frac{1}{2}$: $V_\theta = 3\times10^3$ m s^{-1}. The difficulty with this explanation arises when the 3/1 mode grows during the transition to regime III in which both the 3/1 and 1/1 modes lock together with a common phase and frequency, since this is inconsistent with rigid poloidal rotation.

The second possibility (b) would require only the fairly modest toroidal velocity differential of 8×10^4 ms^{-1} at the $q = 1$ surface ($r_1 \approx 3$ cm) compared with 11×10^4 ms^{-1} at the plasma boundary. However, the problem of mode locking remains.

Thus it would appear that, at least for modes with amplitudes too small for locking to occur, we cannot exclude the possibility that the perturbations can move with respect to the plasma, their velocity thus being superimposed on a (usually) much larger and probably rigid toroidal rotation of the bulk plasma. However, in the absence of accurate independent measurements of bulk rotation this must remain conjectural.

Regime III

The first point of interest here is that the transition into regime III occurs at $q(a) = 2\cdot8$ which corresponds rather precisely with the 'correct' value $q_\psi(a) = 3\cdot0$, i.e. to the plasma boundary becoming resonant to the strongest externally observed mode $m/n = 3/1$, which is thus in direct contact with the limiter.

The rather dramatic change in the SXR emissivity profile shown in Fig. 9 can be shown, taking into account the decrease in electron density, to be consistent with a sudden decrease in central temperature of up to 100 eV, together with some broadening of the profile. The change constitutes a significant worsening of the confinement of both energy and particles. It is also found that high energy runaway electrons are lost from the system during this phase, as evidenced by the sudden increase in hard X-ray emission from the limiter which persists throughout these conditions.

These observations are generally consistent with the widely accepted model in which energy is rapidly transported from the plasma across an island which contacts the limiter. For these conditions we can estimate from equation (3) an island half-width $\delta \sim 8$ mm. It should be noted that despite the fact that the signal from the $m = 2$ array is approximately the same as that from the $m = 3$ array, which would be commonly interpreted as indicating the existence of a strong $m = 2$ mode at the $q = 2$ surface, this would be misleading when compared with a more complete harmonic analysis. The actual shape of the perturbation shown in Fig. 14 makes the dominant 3/1 structure obvious. Since the $q = 3$ surface lies outside the current channel, the observed 3/1 perturbation would take the form of an external kink mode rather than a set of magnetic islands resulting from a tearing mode (Wesson 1978).

The SXR signals provide the only reliable information about the internal modes. Fig. 15 shows typical minor radial variation of SXR signals A, their peak-to-peak fluctuation amplitude $\tilde{A}$, together with their relative phase ϕ (obtained from Fourier analysis) and normalized amplitude $\tilde{A}/A$. Unfortunately this type of chordal observation makes unambiguous determination of the poloidal mode number very difficult (other than $m = 1$ which is clear from Fig. 15). In this instance they appear to originate from a large rotating $m = 1$ island. From results shown in Fig. 15, we find that the fluctuations are maximum at $r \approx 2 \cdot 5 \pm 0 \cdot 5$ cm, where $q = 1$ is expected, with indications of another peak between 6 and 8 cm which would include r_2 $(q = 2)$. Comparison of the phases of the signals from the two X-ray arrays shows that the toroidal mode has the value $n = 1$. Although the fast oscillations are much larger than the sawteeth variations, Fourier analysis shows that the latter are still present, but are far too weak to define with sufficient accuracy the radius of the inversion layer as in regime I.

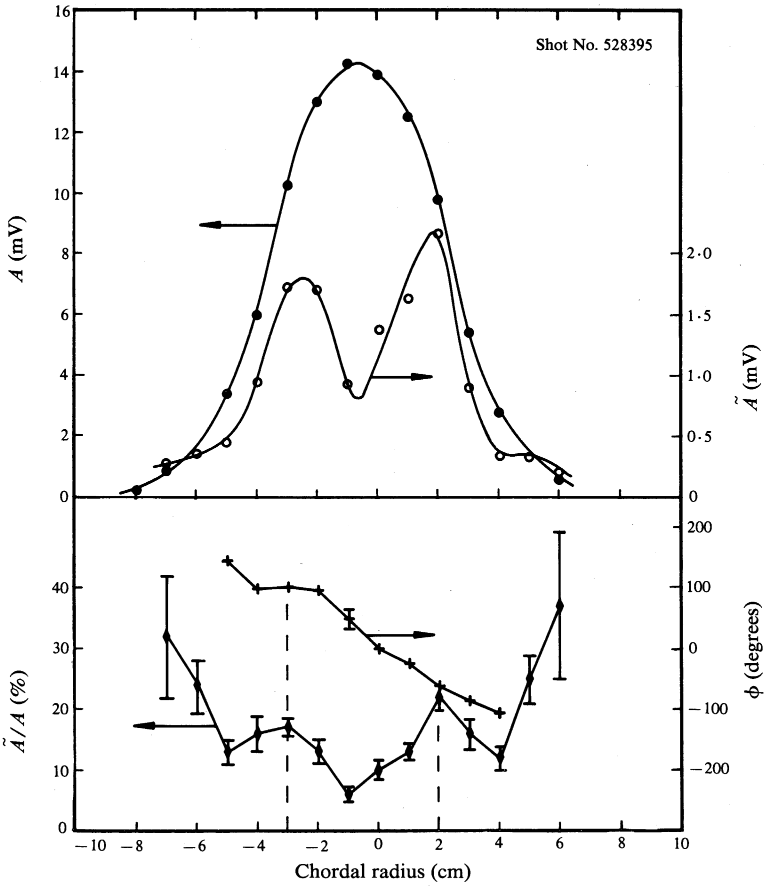

Fig. 15. Soft X-ray data taken during regime III showing the X-ray flux profile A, the peak-to-peak amplitude of the MHD oscillations $\tilde{A}$, the normalized amplitude $\tilde{A}/A$ and the relative phase of the signals obtained from Fourier analysis ϕ.

Thus there appears to be a dominant 1/1 mode which occupies a large part of the central hot plasma region, accompanied by an apparently weaker 2/1 mode farther out in the cooler, more weakly radiating region, which appears to determine the overall plasma behaviour. The close relationship between the internal and external signals, plus the fact that the 3/1 perturbation appears to be located *outside* the current channel in the still highly conducting region in the shadow of the limiter, strongly suggests that the external signals are actually *driven* nonlinearly by the 1/1 mode (Carreras *et al.* 1983; Tsuji *et al.* 1985), rather than arising from a local instability.

Because very distinct magnetic signals are obtained in this regime, it was used to investigate any clear dependence of the observed frequency. In addition to the operation being extended over the appreciable parameter range listed in Section 3, the observations were repeated in both helium and argon. This allowed us to to explore the possibility, for example, of any ion mass dependence as well as including several very different plasma conditions. Regardless of these considerable changes, the frequency remained between 12 and 25 kHz. Apart from the general trend that the frequency decreased as the amplitude increased, the actual results were not reproducible in otherwise reproducible discharges, so that no firm conclusions could be drawn, other than the lack of any obvious dependence on ion mass.

Regime IV

This region of operation is again relatively quiescent and strongly resembles regime I. Confinement once more improves as shown by the increase in the total SXR emission, while increasing the gas flow rate during these conditions allows the density to be increased through the $q = 3$ window up to limits determined by the maximum gas flow. [On the basis of experience elsewhere (FT Group 1983) we should have expected to significantly increase the plasma density in this regime if a longer pulse duration had been available.]

The SXR profile remains broad, with the $q = 1$ surface appearing at a slightly greater radius than in regime I. Once again, the only well-defined activity is the 1/1 internal mode superimposed on the sawteeth, with only quite weak magnetic signals observed.

As mentioned earlier, it is from these rather quiet and well-behaved conditions that the low-q major disruptions develop, apparently without the previous growth to large amplitudes of a 2/1 mode, which is usually observed to occur in most other tokamaks just before disruption (see e.g. TFR Group 1977). This aspect will be reported and discussed more fully elsewhere.

It should be noted that the behaviour of the plasma, in particular its propensity to disrupt, depends critically on the impurity level, and thus, by implication, on the precise q profile.

5. Summary and Conclusions

As a result of the extensive experimental investigations of the MHD activity detailed above we draw some general conclusions.

(i) The main features of the activity can be classified into four main types or regimes which depend almost entirely on the value $q(a)$, which are almost independent of the main plasma parameters and which vary only slightly with vacuum conditions.

(ii) Despite all attempts to influence the observed frequency in a controlled manner by changing plasma conditions, no systematic dependence has been found.

(iii) Although under most circumstances all observable modes appear to be phase-locked together at a common frequency, consistent with rigid toroidal rotation of the plasma, under some conditions the outermost mode appears at a substantially different and incommensurate frequency from the others. This behaviour is consistent with the superposition of a small poloidal velocity onto the rigid toroidal rotation, a non-rigid, sheared toroidal rotation, or the movement of the outer mode with respect to the bulk medium.

(iv) For $q(a) < 2{\cdot}5$ only those modes inside the plasma associated with the $q = 1$ surface have significant amplitude, the outer regions showing only weak activity. This differs markedly with results from other tokamaks in which strong $m = 2$ activity is observed for $q(a) < 3$, growing to large amplitude just before disruption.

Acknowledgments

The authors would like to thank the technical staff of the laboratory for their work in keeping LT-4 and its systems in good running order, in particular D. Vender for operating the tokamak, G. C. J. Davies and R. J. Kimlin for their close support of the electronics, and G. McCluskey and the Homopolar Generator team. We would also like to thank G. R. Hogg for his contributions to the X-ray measurements and M. A. Corbould and C. F. Vance for their work on the computing and data acquisition systems.

We also acknowledge financial assistance from the Australian Atomic Energy Commission, the Australian Institute of Nuclear Science and Engineering and the National Energy Research, Development and Demonstration Program of the Department of Resources and Energy.

References

Bateman, G. (1978). 'MHD Instabilities' (MIT Press).

Bell, M. G., Cheetham, A. D., Hamberger, S. M., Hogg, G. R., Hollis, M. J., How, J. A., Kuwahara, H., Morton, A. H., Sharp, L. E., Whitbourn, L. B., and Vance, C. F. (1984). *Aust. J. Phys.* **37**, 137.

Bowers, D. L., Liley, B. S., Morton, A. H., and Vance, C. F. (1971). *Plasma Phys.* **13**, 849.

Carreras, B. A., *et al.* (1983). MHD activity in the ISX-B tokamak: Experimental results and theoretical interpretation. Oak Ridge National Laboratory Rep. No. ORNL/TM-8648.

Cheetham, A. D., Hamberger, S. M., Hogg, G. R., How, J. A., Kuwahara, H., Morton, A. H., Sharp, L. E., and Vance, C. F. (1983). Proc. 11th European Conf. on Controlled Fusion and Plasma Physics, Aachen (Ed. S. Methfessel), Part 1, p. 81 (European Physical Society: Julich).

Cheetham, A. D., Hamberger, S. M., How, J. A., Kuwahara, H., Morton, A. H., Sharp, L. E., and Vance, C. F. (1985). *In* 'Plasma Physics and Controlled Nuclear Fusion Research', Vol. I, p. 337 (IAEA: Vienna).

Corbould, M. A., and How, J. A. (1984). *Comput. Phys. Commun.* **32**, 231.

Fielding, S. J., Hugill, J., McCracken, G. M., Paul, J. W. M., Prentice, R., and Stott, P. E. (1977). *Nucl. Fusion* **17**, 1382.

FT Group (1983). Proc. 11th European Conf. on Controlled Fusion and Plasma Physics, Aachen (Ed. S. Methfessel), Part 1, p. 27 (European Physical Society: Julich).

Furth, H. P. (1975). *Nucl. Fusion* **15**, 487.

Furth, H. P., Killeen, J., and Rosenbluth, M. N. (1963). *Phys. Fluids* **6**, 459.

Hassan, A. B., and Kulsrud, R. M. (1978). *Phys. Fluids* **21**, 2271.

Hosea, J. C., Bobeldijk, C., and Grove, D. J. (1971). Proc. 4th IAEA Conf. on Plasma Physics and Controlled Nuclear Fusion Research, Madison. Vol. II, p. 425 (IAEA: Vienna).

Knoepfel, H., and Spong, D. A. (1979). *Nucl. Fusion* **19**, 785.

Kuwahara, H., Cheetham, A. D., Hamberger, S. M., Hogg, G. R., Morton, A. H., and Sharp, L. E. (1983). Proc. IEEE Int. Conf. on Plasma Science, p. 54 (IEEE: San Diego).

Mirnov, S. V., and Semenov, I. B. (1971). *Sov. Phys. JETP* **33**, 1134.

Stix, T. H. (1976). *Phys. Rev. Lett.* **36**, 521.

TFR Group (1977). *Nucl. Fusion* **17**, 1283.

TFR Group (1982). Minor and major disruptions in TFR. Rep. No. EUR-CEA-FC-1151.

Thyagaraja, A., and Haas, F. A. (1983). *Plasma Phys.* **25**, 459.

Tsuji, S., Nagayama, Y., Miyamoto, K., Kawahara, K., Noda, N., and Tanahashi, S. (1985). *Nucl. Fusion* **25**, 305.

Turner, M. F., and Wesson, J. A. (1982). *Nucl. Fusion* **22**, 1069.

Von Goeler, S., Stodiek, W., and Suathoff, N. (1974). *Phys. Rev. Lett.* **33**, 1201.

Waddell, B. V., Carreras, B., Hicks, H. R., and Holmes, J. A. (1979). *Phys. Fluids* **22**, 896.

Wesson, J. A. (1978). *Nucl. Fusion* **18**, 87.

Wing, W. (1975). *In* 'Course on Plasma Diagnostics and Data Acquisition Systems' (Eds A. Eubank and E. Sindoni), p. 324 (CNR–EURATOM: Bologne).

Manuscript received 25 July, accepted 22 October 1985